

Phase behavior and percolation in an equilibrium system of symmetrically interacting Janus disks on the triangular lattice

Xixian Zhang(张希贤) and Hao Hu(胡皓)

Citation: Chin. Phys. B, 2023, 32 (**8**): 080502. DOI: 10.1088/1674-1056/acc7fe
Journal homepage: http://cpb.iphy.ac.cn; http://iopscience.iop.org/cpb

What follows is a list of articles you may be interested in

Universal order-parameter and quantum phase transition for two-dimensional *q*-state quantum Potts model

Yan-Wei Dai(代艳伟), Sheng-Hao Li(李生好), and Xi-Hao Chen(陈西浩)
Chin. Phys. B, 2022, 31 (**7**): 070502. DOI: 10.1088/1674-1056/ac4bd1

Dynamical quantum phase transition in *XY* chains with the Dzyaloshinskii-Moriya and *XZY-YZX* three-site interactions

Kaiyuan Cao(曹凯源), Ming Zhong(钟鸣), and Peiqing Tong(童培庆)
Chin. Phys. B, 2022, 31 (**6**): 060505. DOI: 10.1088/1674-1056/ac4a6e

Dynamic phase transition of ferroelectric nanotube described by a spin-1/2 transverse Ising model

Chundong Wang(王春栋), Ying Wu(吴瑛), Yulin Cao(曹喻霖), and Xinying Xue(薛新英)
Chin. Phys. B, 2021, 30 (**2**): 020504. DOI: 10.1088/1674-1056/abbbfd

Topological Anderson insulator in two-dimensional non-Hermitian systems

Hongfang Liu(刘宏芳), Zixian Su(苏子贤), Zhi-Qiang Zhang(张智强), Hua Jiang(江华)
Chin. Phys. B, 2020, 29 (**5**): 050502. DOI: 10.1088/1674-1056/ab8201

Hydrophobic nanochannel self-assembled by amphipathic Janus particles confined in aqueous nano-space

Gang Fang(方钢), Nan Sheng(盛楠), Tan Jin(金坦), Yousheng Xu(许友生), Hai Sun(孙海), Jun Yao(姚军), Wei Zhuang(庄巍), Haiping Fang(方海平)
Chin. Phys. B, 2018, 27 (**3**): 030505. DOI: 10.1088/1674-1056/27/3/030505

Phase behavior and percolation in an equilibrium system of symmetrically interacting Janus disks on the triangular lattice

Xixian Zhang(张希贤)[1,2] and Hao Hu(胡皓)[1,†]

[1] *School of Physics and Optoelectronic Engineering, Anhui University, Hefei* 230601, *China*
[2] *School of Materials Science and Engineering, Anhui University, Hefei* 230601, *China*

(Received 2 January 2023; revised manuscript received 6 March 2023; accepted manuscript online 28 March 2023)

A Janus particle has two distinct areas on its surface. Denoting the two areas as P (patch) and N (nonpatch), when two particles come close to each other, the strength of the PP interaction is usually different from that of the NN interaction. Recently the interplay between a rotational-symmetry-breaking continuous phase transition and percolation has been explored for an equilibrium system of asymmetrically interacting (i.e., attractive PP interaction, zero NN and PN interactions) Janus disks on the triangular lattice. By Monte Carlo simulation and finite-size scaling analysis, in this work we study an equilibrium system of symmetrically interacting (i.e., attractive PP and NN interactions with the same strength, zero PN interaction) Janus disks on the same lattice. By definition, the phase diagram in the T–θ plane is symmetric for systems with patch sizes θ below and above 90°. We determine the phase diagram and compare it with that of the asymmetric system. Similar to the latter system, for $60^\circ < \theta < 90^\circ$, a rotational-symmetry-breaking continuous phase transition and an anisotropic percolation transition are found in the symmetric system, though the transition points in the two systems are quite different. Phase crossover curves are found to be different, e.g., a continuous varying crossover line extends between $\theta = 0^\circ$ and 90° for the symmetric model; and in the range $0^\circ < \theta \leq 30^\circ$, along the crossover lines of the two models, the trends of $1/T$ vs. θ are opposite in the two systems. We understand the latter by analytically solving the models with two particles in $0^\circ < \theta \leq 30^\circ$. These results are helpful for understanding close-packed systems of Janus disks with more complex interactions.

Keywords: Janus particles, phase transitions, percolation, Monte Carlo methods

PACS: 05.70.Fh, 05.10.Ln, 82.70.Dd, 64.60.ah **DOI:** 10.1088/1674-1056/acc7fe

1. Introduction

Janus particles have two surface areas with different properties.[1,2] The inhomogeneity of particle surfaces lead to anisotropic interactions between Janus particles. The unique interactions give many research opportunities in soft matter physics and materials sciences,[3–6] such as the self-assembly of entropy-stabilized open lattices[7,8] and orientationally ordered crystals.[9–11] Recently, there have been many works which study close-packed Janus systems in two dimensions (2D), focusing on melting,[12,13] orientational dynamics,[9,14] phase transitions and crossovers,[12,14–20] and percolation,[20,21] etc.

In equilibrium triangular-lattice simulations of a model of close-packed Janus disks, Mitsumoto and Yoshino[14] found a continuous phase transition which breaks a three-fold rotational symmetry for patch sizes (defined in Section 2) $60^\circ < \theta < 90^\circ$, and two kinds of crossovers between different structures for $\theta < 60^\circ$. In this Janus system, there is an attractive interaction between contacting patches on two neighboring particles (denoted as PP interaction), and other types of interactions contribute zero energy. The continuous phase transition is from a high-T disordered phase to a low-T orientationally ordered stripe phase. In the same system, we previously found that percolation in the stripe phase is anisotropic since the critical clusters are longer in the direction parallel to the stripes than in the perpendicular direction.[20] It is shown that universal critical properties of anisotropic percolation in the Janus system can be explained by standard isotropic percolation through a nontrivial spatial rescaling, which can be generalized to understand percolation in other anisotropic systems, such as bond percolation with anisotropic bond-placing rules, and Potts models with various couplings in different directions.

From the phase diagram in Ref. [20], it can be seen that, for $\theta > 90^\circ$, there is also a continuous phase transition which beaks a three-fold rotational symmetry. The stable region of the stripe phase for $\theta > 90^\circ$ is much narrower along the θ axis than that for $\theta < 90^\circ$. This could be attributed to the asymmetric nature of the two-particle interaction, i.e., there is an attractive PP interaction when two particles contact via patches, while the energy is zero when they contact via nonpatches (NN interaction is zero). However, it remains unclear how the phase behavior and percolation would change if an attractive NN interaction is introduced between neighboring particles in the system.

In this work, by Monte Carlo simulations and finite-size scaling analysis, we study a symmetrically interacting Janus system with equal attractive PP and NN interactions, and com-

†Corresponding author. E-mail: huhao@ahu.edu.cn

© 2023 Chinese Physical Society and IOP Publishing Ltd

pare it with the above asymmetrically interacting system existing an attractive PP interaction and zero NN interaction. We obtain the phase diagram of the symmetric model and get a more complete phase diagram of the asymmetric model. The similarities and differences between the phase behavior and percolation in the two models are presented in detail. These results show the potential of tuning the interactions to design the phase diagram, and could provide useful references for exploring systems with more complex interactions, such as systems with unequal nonzero PP and NN interactions or with nonzero PN interactions.

The rest of this paper is organized as follows. Section 2 illustrates the model and method. Section 3 presents the results, including a summary of the phase diagrams and an analysis of the ground state in Subsection 3.1, and detailed analysis for different ranges of patch sizes in Subsection 3.2. Finally, in Section 4, we give conclusions and discussion.

2. Model and method

The symmetrically interacting model is a generalization of the asymmetrically interacting model studied in previous works,[14,15,20] which adopt an interacting potential of Kern–Frenkel type.[22] In the models, Janus disks are put on rhombus-shaped triangular lattices under periodic boundary conditions. Each lattice site is occupied by a disk with the disk center fixed at the site. The diameter of a disk is equal to the distance between two nearest-neighboring sites. Thus the disks are close-packed and each disk can only rotate. As shown in Fig. 1, each disk has a patch P which spans an angle of 2θ, and the remaining nonpatch N spans an angle of 360°–2θ. Here the half-patch angle θ characterizes the size of a patch, which is equivalent to the so-called Janus balance that can be tuned in experiments.[23] The direction $\boldsymbol{S}_i$ of a disk i is defined by the arrow connecting the disk center and the patch center. The symmetric model and the asymmetric model are different by their definitions of energies. In the asymmetric model, for two neighboring particles, only when their patches cover the same edge (i.e., the interaction is of PP type), as shown in Fig. 1(a), there is an energy $-\varepsilon$, otherwise the pair energy is zero. The symmetric model is defined by introducing an energy $-\varepsilon$ when nonpatches of two neighboring particles cover the same edge (i.e., the interaction is of NN type), as shown in Fig. 1(b), in addition to the above $-\varepsilon$ PP interaction and zero PN interaction. The total energy E of a system is the summation of all pair energies.

We performed Monte Carlo simulations to investigate equilibrium properties of the models. In simulations, the disks are visited sequentially,[24] and when a disk is being visited, it is proposed to rotate randomly by an angle in the range $[-180^\circ, 180^\circ)$. The Metropolis criterion is employed to accept or reject the proposed move. In each run of the simulation, around 5×10^6 Monte Carlo sweeps (MCSs) were used for the equilibration process. The equilibration time was checked to be much longer than the autocorrelation time. After the equilibration, around 10^7 MCSs were simulated for equilibrium sampling. For observing the phase transition and percolation, we performed 30 statistically independent runs to calculate the means and error bars. For the symmetric model, we simulated lattices with the linear size $L = 16$, 32, 64, and 128, and for the asymmetric model $L = 48$, 72, and 108. Only a few runs and smaller system sizes were employed for observing the crossover behavior.

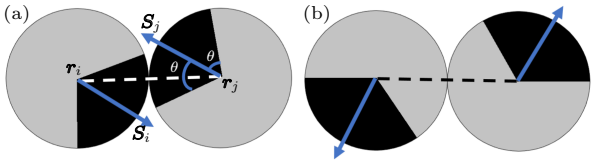


Fig. 1. Schematic representation of Janus disks. Each disk has a patch P which spans an angle of 2θ. The left plot shows an interaction of PP type, and the right plot shows an interaction of NN type, where N stands for nonpatch. In the symmetric model, both PP and NN interactions contribute an energy $-\varepsilon$. In the asymmetric model, the PP interaction has an energy $-\varepsilon$ while the NN interaction has zero energy. A PN interaction has zero energy in both the models.

To observe the thermodynamic phase behavior, we sampled the specific heat, an order parameter and its associated Binder quantity,[14] which are defined as follows. The specific heat is given by

$$C_{\rm e} = (\beta^2/N)[\langle E^2\rangle - \langle E\rangle^2], \tag{1}$$

where $\beta = 1/k_{\rm B}T$, with $k_{\rm B}$ being the Boltzmann constant. For simplicity the unit of T is taken as $\varepsilon/k_{\rm B}$ in the following. Near phase transitions, usually there is a sharp peak in $C_{\rm e}$, which diverges in the thermodynamic limit; while near crossovers, there is a finite broad peak in $C_{\rm e}$, and the $C_{\rm e}$ curves of different system sizes L overlap. We shall use $C_{\rm e}$ to detect the phase transition and crossover points.

An order parameter Ψ is introduced in Ref. [14] to detect the three-fold rotational symmetry breaking. It is defined as $\Psi = (\psi_x, \psi_y)$, with the two components as follows:

$$\begin{aligned}\psi_x &= \frac{\sqrt{3}}{2}[S(\boldsymbol{k}_2) - S(\boldsymbol{k}_3)],\\ \psi_y &= S(\boldsymbol{k}_1) - \frac{1}{2}[S(\boldsymbol{k}_2) + S(\boldsymbol{k}_3)],\end{aligned} \tag{2}$$

which leads to $\Psi^2 = S^2(\boldsymbol{k}_1)+S^2(\boldsymbol{k}_2)+S^2(\boldsymbol{k}_3)-S(\boldsymbol{k}_1)S(\boldsymbol{k}_2)-S(\boldsymbol{k}_2)S(\boldsymbol{k}_3)-S(\boldsymbol{k}_3)S(\boldsymbol{k}_1)$. Here $S(\boldsymbol{k})$ is the static structure factor given by

$$\begin{aligned}S(\boldsymbol{k}) &= \frac{1}{N}\left|\sum_{i=1}^{N} {\rm e}^{{\rm i}\boldsymbol{r}_i\cdot\boldsymbol{k}}\boldsymbol{S}(0)\cdot\boldsymbol{S}(\boldsymbol{r}_i)\right|,\\ \boldsymbol{k} &= \frac{n_1}{L}\boldsymbol{b}_1 + \frac{n_2}{L}\boldsymbol{b}_2,\ \ (n_1, n_2 = 0, 1, 2, \ldots, L-1),\end{aligned} \tag{3}$$

where $\boldsymbol{k}$ is a wave vector, and $\boldsymbol{b}_i$ is a reciprocal vector of the triangular lattice, with $\boldsymbol{b}_1 = 2\pi(1, 1/\sqrt{3})$ and $\boldsymbol{b}_2 = 2\pi(0, 2/\sqrt{3})$.

Three possible orientations of stripes on the triangular lattice can be represented in the reciprocal space by $\boldsymbol{k}_1 = \boldsymbol{b}_1/2$, $\boldsymbol{k}_2 = \boldsymbol{b}_2/2$, and $\boldsymbol{k}_3 = \boldsymbol{b}_1/2 + \boldsymbol{b}_2/2$. The above static structure factor is a Fourier transformation of real-space spin correlations, and it can probe the spin structure order in different $\boldsymbol{k}$ directions. In Fig. 2(c) of Ref. [14] for the asymmetric model, a density plot of $S(\boldsymbol{k})$ in the reciprocal space is shown, and it has high-density spots at $\boldsymbol{k}_1$, $\boldsymbol{k}_2$, and $\boldsymbol{k}_3$.

The absolute value of the order parameter $|\Psi|$ is zero if the three-fold rotational symmetry is preserved, and it changes to nonzero values when the three-fold rotational symmetry is broken. To more precisely determine the phase transition point, we use the following Binder quantity:[14]

$$B = \frac{3}{2}\left(1 - \frac{\langle \Psi^4 \rangle}{3\langle \Psi^2 \rangle^2}\right). \tag{4}$$

In the plot of B vs. T, if the phase transition is continuous, curves for difference system sizes L approximately cross near the phase transition point T_c. For a continuous phase transition, the Binder quantity B can be expressed as

$$B = B_0 + a_1(T_c - T)L^{y_t} + b_1 L^{y_1}, \tag{5}$$

where B_0 represents the value of B in the thermodynamic limit, $y_t = 1/\nu$ is the thermal renormalization exponent, $y_1 < 0$ is a correction exponent coming from the irrelevant scaling field, a_1 and b_1 are non-universal amplitudes.

We also performed percolation studies in the Janus models. In previous works for the asymmetric model,[20,21] percolation of clusters with PP connections was explored: neighboring particles are considered as connected when their interaction is of PP type; clusters grow as the patch size increases or the temperature decreases; and at the percolation threshold an incipient cluster spanning the whole system appears. In this work, we consider percolation of clusters with PP connections in the symmetric model, and also study percolation of clusters with NN connections in both the symmetric and asymmetric models.

We combine Monte Carlo simulations with the critical-polynomial method[25–30] to precisely determine the percolation threshold. For a finite periodic lattice B in 2D, the probabilistic definition[28] of the critical polynomial is

$$P_B \equiv R_2 - R_0, \tag{6}$$

where R_2 is the probability of the percolation configurations being wrapping in two different directions, and R_0 is the probability of being no wrapping. For completeness, we also measure R_1 which is the probability of wrapping in only one direction. Wrapping events are detected by a method[31,32] originally used in simulating Potts models. Assuming the universality of standard percolation in 2D, for percolation in the Janus models at fixed T, the root $\theta(L)$ of $P_B(\theta, L) = 0$ gives an estimate of the percolation threshold, which becomes more accurate as L increases and converges to the percolation threshold θ_p in the limit $L \to \infty$. It is known from previous studies that the critical polynomial can give exact thresholds for solvable lattice percolation problems even when L takes the smallest value applicable,[30] and the threshold converges very rapidly to its infinite-size value for unsolved percolation problems.[30,33] The critical polynomial P_B is a dimensionless quantity, and according to the renormalization group theory, its finite-size scaling behavior is expected to follow the formula[33]

$$P_B(\theta, L) \simeq a_1(\theta - \theta_p)L^{y_t} + b_1 L^{y_1}, \tag{7}$$

where a_1 and b_1 are non-universal amplitudes, $y_t = 1/\nu$ is the thermal renormalization exponent, and $y_1 < 0$ is leading correction exponent. Since the percolation transition is different from the continuous thermodynamic phase transition, the values of exponents are expected to be different from those in Eq. (5).[20]

3. Results

We first present the ground states and phase diagrams, then discuss in detail the phase behavior in different ranges of patch sizes.

3.1. Ground states and phase diagrams

A ground state is the lowest energy state of the model. In ground states, the symmetric model minimize its number of NP interactions, while the asymmetric model maximize its number of PP interactions. We identify the ground states of the symmetric model as plotted in Fig. 2. For $0^\circ < \theta \leq 30^\circ$, a particle can have one PP interaction and five NN interactions with its nearest-neighboring particles, as shown in Fig. 2(a); a particle can also have six NN interactions with its nearest-neighboring particles, as shown in Fig. 2(b). For $30^\circ < \theta \leq 60^\circ$, a particle has two PP interactions and four NN interactions, as plotted in Fig. 2(c) or Fig. 2(d). At finite low temperatures, similar to that for the asymmetric model,[15] a trimer phase consisting of the state in Fig. 2(c) dominates as it has much larger configurational entropy than a stripe phase consisting of the state in Fig. 2(d). For $60^\circ < \theta \leq 90^\circ$, there are two different ground states: one has three PP interactions and three NN interactions, the other has two PP interactions and four NN interactions. Figures 2(e) and 2(f) show these two states, which both assemble into stripes as illustrated in Figs. 2(g) and 2(h), respectively. Since the range $90^\circ \leq \theta < 180^\circ$ is symmetric to the range $0^\circ < \theta \leq 90^\circ$ around $\theta = 90^\circ$, the ground states of the former are those of the latter with the P and N areas interchanged.

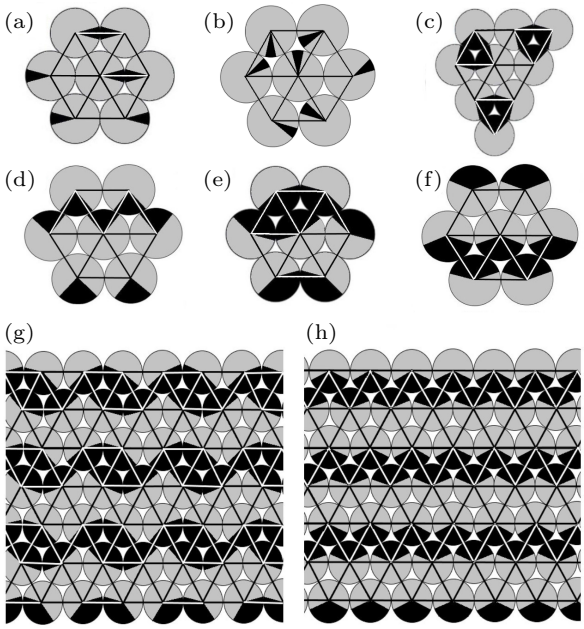


Fig. 2. The ground states of the symmetric model in different ranges of patch sizes: [(a), (b)] $0^\circ < \theta \leq 30^\circ$, [(c), (d)] $30^\circ < \theta \leq 60^\circ$, [(e), (f)] $60^\circ < \theta \leq 90^\circ$. States in (e) and (f) assemble into orientationally ordered stripes as shown in (g) and (h), respectively. A white bond represents a PP interaction and a black bond represents an NN interaction.

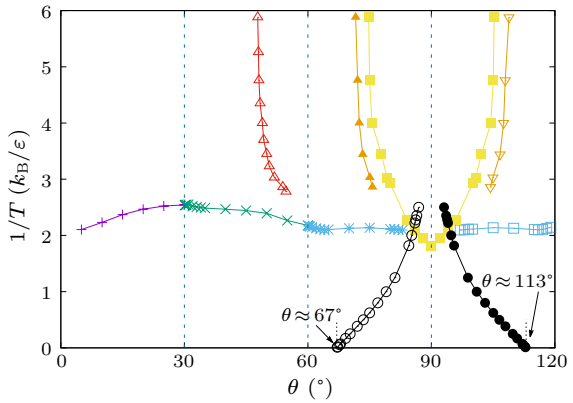


Fig. 3. Phase diagram of the symmetric model on the triangular lattice. The diagram is symmetric around $\theta = 90^\circ$, and for brevity the range $120^\circ < \theta \leq 180^\circ$ is not plotted. Solid squares represent a line of continuous phase transition, across which the system transform from a high-T disordered phase to a low-T orientationally ordered stripe phase. Lines with circles indicate the percolation transition: to the left side of the empty circles the system is percolated with NN connections, and to the right side of the solid circles it is percolated with PP connections. All other lines indicate phase crossovers.

For the asymmetric model, since the strength of NN interactions is zero, its ground states[15] are similar but different. For $0^\circ < \theta \leq 30^\circ$, the ground state consists of dimers as shown in Fig. 2(a). For $30^\circ < \theta \leq 60^\circ$, the ground states are shown in Figs. 2(c) and 2(d), as the same as those of the symmetric model. For $60^\circ < \theta \leq 90^\circ$, the ground state is Fig. 2(e). For $90^\circ < \theta \leq 120^\circ$, the ground state is Fig. 2(f) with P and N areas interchanged.

After analyzing the ground states, by Monte Carlo simulations and finite-size scaling analysis, we determine the phase diagram of the symmetric model as shown in Fig. 3, and compare it with that of the asymmetric model as plotted in Fig. 4. There are mainly two sets of results: (i) in the range $60^\circ < \theta \leq 120^\circ$, both the models have a line of continuous phase transitions, separating a high-T disordered phase from a low-T orientationally ordered stripe phase, and both of them have two lines of percolation transitions: one for clusters with PP connections and the other for clusters with NN connections. However, while these transition lines are symmetric around $\theta = 90^\circ$ for the symmetric model by definition, they appear very asymmetric in the asymmetric model. These indicate that tuning the asymmetry of the interactions is a very useful tool to design the stable region of the stripe phase and the connectivity of the systems. (ii) The phase crossover behavior of the symmetric model is found to be very different from that of the asymmetric model. For example, there is a smooth phase-crossover line which spans the range $0^\circ < \theta < 90^\circ$ in Fig. 3 for the symmetric model, while for the asymmetric model different phase-crossover lines in Fig. 4 do not connect near $\theta = 30^\circ$ or 60°. Moreover, the monotonicity of phase-crossover lines could be different in the two models, e.g., in the range $0^\circ < \theta \leq 30^\circ$. A thorough investigation of the phase behavior is presented in the following subsections.

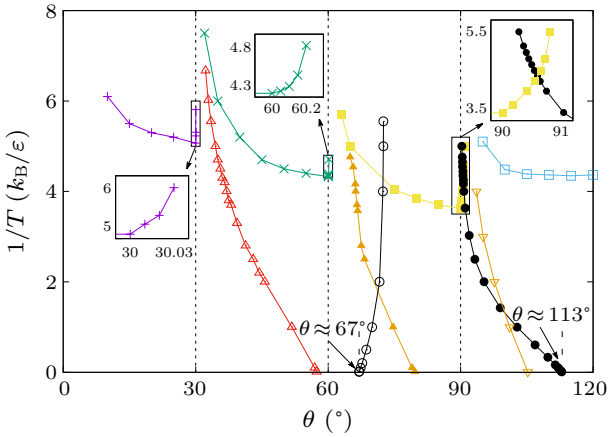


Fig. 4. Phase diagram of the asymmetric model on the triangular lattice. Solid squares represent a line of continuous phase transition, across which the system transforms from a high-T disordered phase to a low-T orientationally ordered stripe phase. Lines with circles indicate the percolation transition: to the left side of the empty circles the system is percolated with NN connections, and to the right side of the solid circles it is percolated with PP connections. All other lines indicate phase crossovers. The two phase crossover lines with crosses (+ or ×) and the continuous phase transition line in the range $60^\circ < \theta \leq 90^\circ$ appear as the same as those in Ref. [14], except that in this reference the phase crossover slightly above $\theta = 30^\circ$ and 60° is not studied. In the range $90^\circ < \theta \leq 120^\circ$, the continuous phase transition line and the percolation line have been studied in Ref. [20].

3.2. Results for $60^\circ < \theta \leq 120^\circ$

3.2.1. Continuous thermodynamic phase transition

For the asymmetric model, a line of continuous thermodynamic phase transition was previously found both in the range $60^\circ < \theta \leq 90^\circ$[14] and in the range $90^\circ < \theta \leq 120^\circ$.[20] The transitions are from a high-T disordered phase to a low-T orientationally ordered stripe phase, for which ground states are presented in the above subsection. To two sides of $\theta = 90^\circ$,

the transition lines appear to be very asymmetric, as plotted in Fig. 4.

For the symmetric model, we find a similar continuous thermodynamic phase transition from the disordered phase to the stripe phase, and determine the transition line as shown in Fig. 3. By definition, the phase diagram in the range $60^\circ < \theta \leq 120^\circ$ is symmetric around $\theta = 90^\circ$. In the following, the system with $\theta = 90^\circ$ is used to illustrate the phase-transition properties, which are found to be similar to those for the system with other θ values within $90^\circ \pm 30^\circ$.

As plotted in Fig. 5(a) for the system with $\theta = 90^\circ$, near $T \simeq 0.55$, the specific heat C_e tends to diverge as the system size L increases, which indicates a thermodynamic phase transition. The continuous variation of the order parameter in Fig. 5(b) shows that the transition is continuous, which is further confirmed by the approximate crossing of the Binder quantity near $T \simeq 0.55$ in Fig. 5(c). To precisely estimate the transition temperature T_c, we perform nonlinear least-square fits to the simulation data of the Binder quantity according to Eq. (5). The fit results are summarized in Table 1, from which we estimate $T_c = 0.5508(2)$, $y_t = 1.05(3)$, and $B_0 = 0.723(4)$.

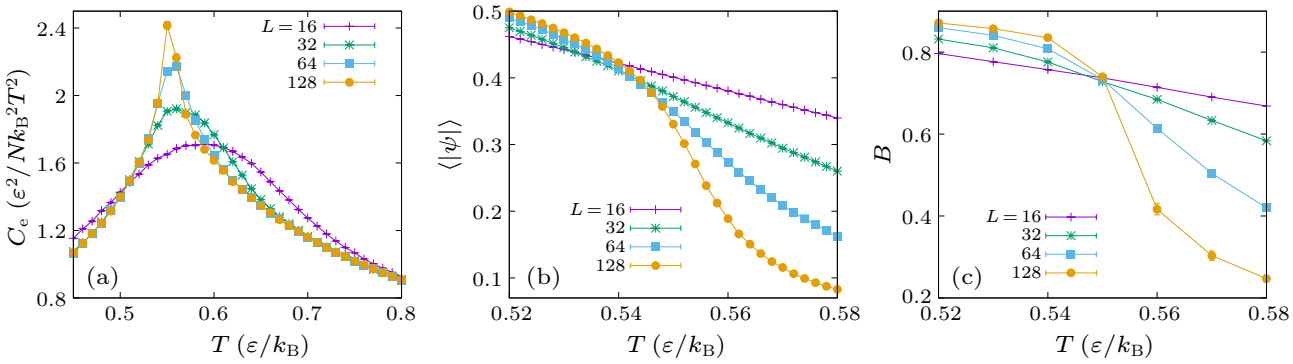


Fig. 5. Simulation results for the symmetric model with $\theta = 90^\circ$: (a) the specific heat C_e vs. T, (b) the order parameter $\langle|\Psi|\rangle$ vs. T, (c) the Binder quantity B vs. T.

Table 1. Fit results of the Binder quantity B for the symmetric model with $\theta = 90^\circ$. A lower cut-off size L_{min} is taken to exclude finite-size corrections not considered in the fit formula. DOF: degree of freedom in the fit.

L_{min}	χ^2/DOF	T_c	B_0	a_1	y_t	b_1	y_1
16	2.7/6	0.55079(9)	0.723(2)	0.123(9)	1.053(19)	0.3(2)	−1.2(3)
16	3.3/7	0.55087(4)	0.7219(5)	0.125(9)	1.050(19)	0.187(6)	−1
32	2.6/4	0.55082(8)	0.722(1)	0.125(15)	1.049(29)	0.16(3)	−1
16	5.8/7	0.55066(3)	0.7267(3)	0.121(9)	1.059(19)	1.87(6)	−2
32	2.6/4	0.55075(6)	0.7253(9)	0.125(15)	1.049(29)	3.0(6)	−2

Considering the universality class of the continuous thermodynamic phase transition, for the asymmetric model, it was suggested in Ref. [14] that the transition belongs to the universality class of the 3-state Potts model in 2D, which was supported by approximate data collapse using critical exponents of the latter model. However, as mentioned in the supplemental material of Ref. [20], it is still possible that the transition belongs to another universality class, since it breaks a Z_3 rotational symmetry instead of a S_3 permutational symmetry broken in the phase transition of the 3-state Potts model. In this work, for the symmetric model, the above fit results suggest $y_t = 1/\nu \simeq 1.05$, which is different from the value $6/5$ for the 3-state Potts model. The transition for the symmetric model also breaks a Z_3 rotational symmetry. Thus, for the symmetric model, it also remains to be explored whether the transition belongs to another universality class or the deviation of the critical exponent from the 3-state Potts value comes from finite-size effects.

3.2.2. Anisotropic percolation behavior

For the asymmetric model, in Ref. [20], for clusters with PP connections, a line of percolation transitions (i.e., thresholds θ_p^{PP} as a function of $1/T$) was found, also as shown by solids circles in Fig. 4. We first consider percolation of clusters with NN connections in the asymmetric model. Percolation thresholds θ_p^{NN} are determined by the critical-polynomial method and plotted as the line with blank circles in Fig. 4. When the temperature is very high, the disks rotate randomly, thus the obtained percolation threshold $\theta_p^{NN} \simeq 67^\circ$ is symmetric to the value $\theta_p^{PP} \simeq 113^\circ$ [the precise value of θ_p^{PP} in the limit $T \to \infty$ is $\theta_p^{PP} = 112.997\,774(5)^\circ$].[21] However, as the temperature drops, θ_p^{NN} approaches $\theta = 90^\circ$, much slower than θ_p^{PP}. Though the line of θ_p^{NN} in Fig. 4 is still far from $\theta = 90^\circ$, we conjecture that it would approach $\theta = 90^\circ$ in the low-T limit, instead of going over $\theta = 90^\circ$. The latter is supported by an observation on the average number of NN connections of a single particle with its neighbors: this number n_b increases with decreasing temperature, and slowly goes to the value 3 as

shown in Fig. 6, which is far over $n_b = 2$ in the ground state of the asymmetric model in the range $90^\circ < \theta \leq 120^\circ$. A similar observation on the number of PP connections along the line of θ_p^{PP} was made in the supplemental material of Ref. [20].

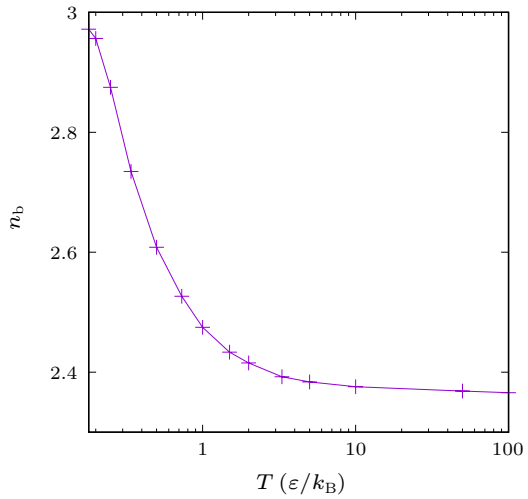


Fig. 6. The average number of NN connections n_b of a single particle vs. T, for the asymmetric model along the percolation line $\theta_p^{NN}(1/T)$.

We then consider percolation in the symmetric model. Two curves of percolation transitions are found, as plotted in Fig. 3, where the curves with blank and solid circles are for clusters with NN connections and PP connections, respectively. The two curves are symmetric to each other due to the symmetry in the definition of the model. Along the percolation line, similar to that for the asymmetric model,[20] critical exponents are found to be consistent with those of standard percolation in 2D, as demonstrated by Figs. 7 and 8 for the disordered and stripe phases, respectively. In Ref. [20] for the asymmetric model, anisotropic critical percolation behavior has been found in the stripe phase, i.e., the critical clusters extend longer in the direction parallel to the stripes than those in the perpendicular direction. After rescaling the parallel direction by a nontrivial effective aspect ratio ρ_e,[20] the configuration becomes isotropic and critical percolation properties can be understood by standard isotropic percolation. Along the percolation line in the stripe phase, it is found that ρ_e changes continuously, resulting in continuously varying dimensionless quantities.[20] We also find such anisotropic behavior in the stripe phase of the symmetric model. Figure 9 shows critical wrapping probabilities along the percolation line of the symmetric model. It can be seen that indeed in the stripe phase ($T \lesssim 0.48$) they vary continuously. It is expected that one can also numerically derive values of ρ_e from these wrapping probabilities[20] to understand the critical anisotropic percolation behavior in the symmetric model.

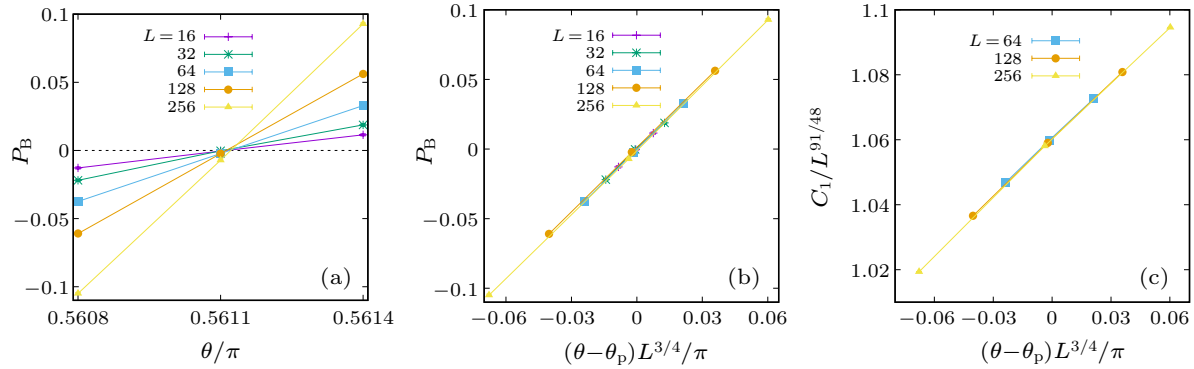


Fig. 7. Percolation in the disordered phase of the symmetric model at $T = 1$. (a) Curves of the critical polynomial P_B at different sizes cross well near the percolation threshold $\theta_p^{PP}/180^\circ = 0.5611$. (b) Data of P_B can be collapsed using the thermal renormalized exponent $y_t = 1/\nu = 3/4$ for standard percolation. (c) Data of the size of largest cluster C_1 can be collapsed using $y_t = 3/4$ and the fractal dimension $d_f = 91/48$ for standard percolation.

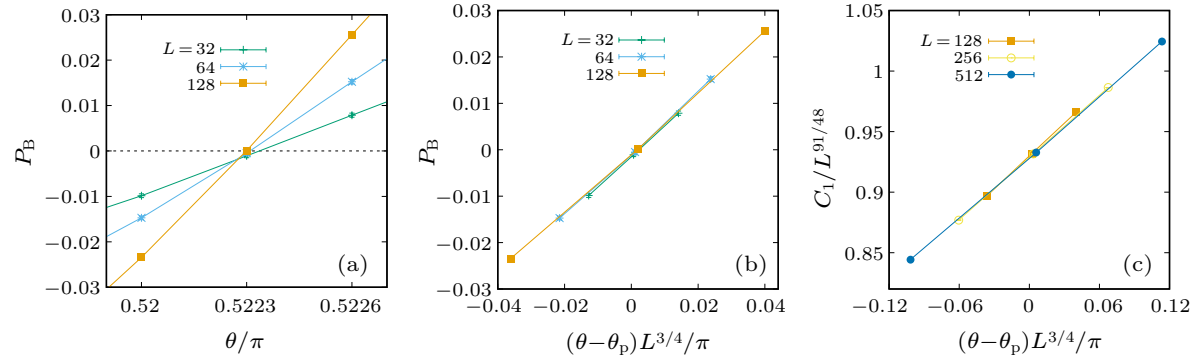


Fig. 8. Percolation in the orientationally ordered stripe phase of the symmetric model at $T = 0.45$. (a) Curves of the critical polynomial P_B at different sizes cross well near the percolation threshold $\theta_p^{PP}/180^\circ = 0.5223$. (b) Data of P_B can be collapsed using the thermal renormalized exponent $y_t = 1/\nu = 3/4$ for standard percolation. (c) Data of the size of largest cluster C_1 can be collapsed using $y_t = 3/4$ and the fractal dimension $d_f = 91/48$ for standard percolation.

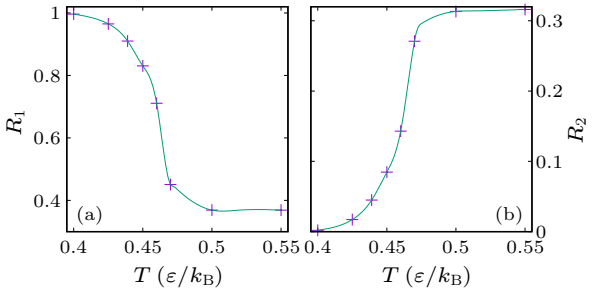


Fig. 9. Critical wrapping probabilities along the percolation line of the symmetric model: (a) R_1 vs. T, (b) R_2 vs. T.

3.2.3. Crossover behavior

For the asymmetric model, in Ref. [20] (i.e., Fig. S1 in the supplemental material of Ref. [20]), when fixing the temperature at $T = 0.25$ and varying the patch size, we found a broad peak of the specific heat C_e which does not depend on the system size, near $\theta/180^\circ = 0.52$ in the disordered phase. The peak signals crossover between a region consisting of many NN-trimers and slightly longer NN-polymers ($\theta/180^\circ > 0.52$) and a region with much less NN-trimers, more monomers and NN-dimers ($\theta/180^\circ < 0.52$), as plotted in Fig. S2 in the supplemental material of Ref. [20]. Fixing T at different values and varying the patch size, we determine a curve of this crossover as shown by blank triangles in the region $90^\circ < \theta < 120^\circ$ in Fig. 4. When fixing the patch size θ and varying the temperature, we also find a broad peak of C_e in the disorder phase, as exemplified in Fig. 10 for $\theta = 105^\circ$. Fixing θ at different values and varying T, we determine a new crossover curve $\theta(1/T)$ as shown by blank squares in the region $90^\circ < \theta < 120^\circ$ in Fig. 4. This curve separates a region mainly consisting of NN-trimers and a region consisting of many NN-trimers and slightly longer NN-polymers. Figure 11 illustrates typical configurations of the three regions separated by the two crossover curves in the disordered phase between 90° and 120°, at $\theta = 100^\circ$.

For the asymmetric model in the disordered phase in the region $60^\circ < \theta < 90^\circ$, we also find two crossover curves, which are shown by solid triangles and cross points in Fig. 4. The curve with crosses is obtained by calculating C_e at varying temperatures for fixed patch sizes. It separates a high-T region dominated by monomers and PP-dimers from a low-T region dominated by PP-trimers, as plotted in Fig. S1 in the supplemental material. The curve with solid triangles is obtained by varying the patch sizes at fixed temperatures, and it indicates a crossover from a region having many small PP-polymers to a region having many longer PP-polymers, as illustrated in Figs. S2(d) and S2(c) in the supplemental material.

For the symmetric model, we also find two crossover curves in the range $60^\circ < \theta < 90^\circ$, as shown in Fig. 3. The curve with crosses is obtained by varying the temperature at fixed patch sizes. It separates a low-T region dominated by PP-trimers from a high-T region with much less PP-trimers and many small PP-clusters of other sizes, as exemplified in Fig. S3 in the supplemental material. The curve with solid triangles is obtained by varying the patch sizes at fixed temperatures, and it indicates a crossover from a region with many small PP-polymers to a region with less small PP-polymers, as illustrated in Figs. S4(d) and S4(c) in the supplemental material.

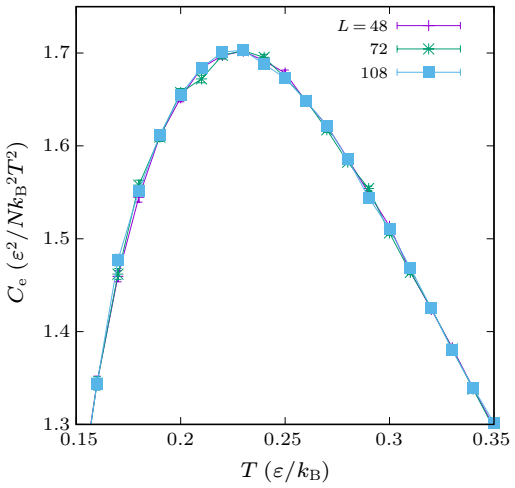


Fig. 10. The specific heat C_e vs. T for the asymmetric model at $\theta = 105^\circ$.

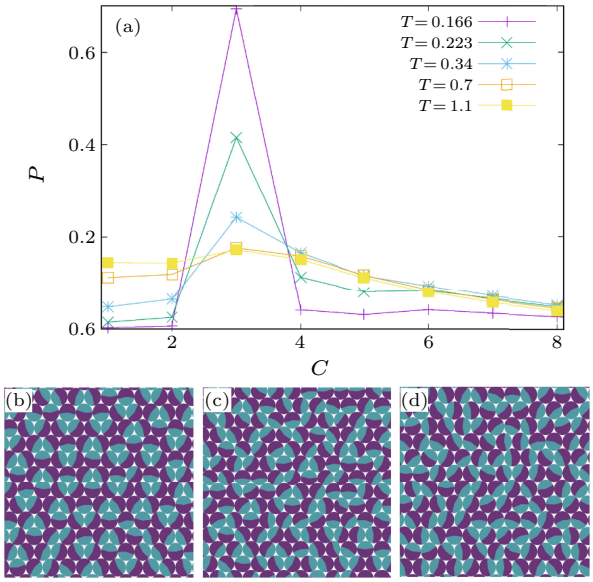


Fig. 11. Results illustrating the crossover behavior in the asymmetric model at patch size $\theta = 100^\circ$ and $L = 72$. (a) Fraction P of disks belonging to clusters of size C with NN connections. Example configurations at (b) $T = 0.166$, (c) $T = 0.34$, and (d) $T = 1.1$. Here $T \simeq 0.223$ and 0.7 are the lower and higher crossover temperatures, respectively.

3.3. Results for $30^\circ < \theta \leq 60^\circ$

In this region of θ, there is no symmetry-breaking phase transition but crossover behavior. For the asymmetric model, as shown in Fig. 4, there are three crossover curves in $30^\circ < \theta \leq 60^\circ$. The curve with tilted crosses (×) was previously found in Ref. [14], as a crossover from a low-T region dominated by PP-trimers to a high-T region with less PP-trimers and many small PP-polymers of other sizes. We find the other

two crossover curves. The curve with crosses (+) is obtained by varying the temperature at fixed patch sizes. It separates a high-T region dominated by monomers from a low-T region dominated by PP-dimers, as plotted in Fig. S5 in the supplemental material. The curve with blank triangles is obtained by varying the patch size at fixed temperatures. It separates a high-T region dominated by monomers and PP-dimers from a low-T region with many PP-trimers and small PP-polymers of other sizes, as plotted in Fig. S6 in the supplemental material.

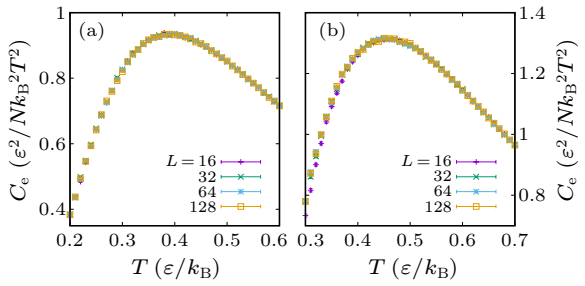


Fig. 12. The specific heat C_e vs. T for the asymmetric model, example specific heat at (a) $\theta = 30^\circ$ and (b) $\theta = 60^\circ$. The broad peak represents a crossover.

For the symmetric model, as shown in Fig. 3, we find two crossover curves in the range $30^\circ < \theta \leq 60^\circ$. The curve with crosses is obtained by varying the temperature at fixed patch sizes. It separates a low-T region dominated by PP-dimers but still with some PP-trimers from a high-T region with less PP-dimers and many monomers, as exemplified for $\theta = 35^\circ$ in Fig. S7 in the supplemental material. The curve with blank triangles is obtained by varying the patch size at fixed temperatures, and it indicates a crossover from a region dominated by PP-dimers to a region dominated by PP-trimers and some longer PP-polymers, as exemplified in Fig. S8 in the supplemental material.

3.4. Results for $0^\circ < \theta \leq 30^\circ$

In this region of θ, there is also no symmetry-breaking phase transition but crossover behavior. For the asymmetric model, as shown in Fig. 4, there is one crossover curve. The curve is obtained by varying the temperature at fixed patch sizes, and it was previously found in Ref. [14], as a crossover from a low-T region dominated by PP-dimers to a high-T region dominated by monomers, as illustrated for $\theta = 20^\circ$ in Fig. S9 in the supplemental material.

For the symmetric model, we also find a crossover curve in the range $0^\circ < \theta \leq 30^\circ$, as shown in Fig. 3. The curve is also obtained by varying the temperature at fixed patch sizes. When the patch size is close to $\theta = 30^\circ$, the curve separates a high-T region dominated by monomers from a low-T region dominated by PP-dimers, as exemplified for $\theta = 25^\circ$ in Fig. S10 in the supplemental material. However, when the patch size is much smaller, since the low-T region is dominated by particles with six NN connections as plotted in Fig. 2(b), the system mainly consists of monomers in both the high-T and low-T regions, as shown for $\theta = 10^\circ$ in Fig. 13(a). The crossover associates with slight change of the number of PP-dimers and monomers, as exemplified in Fig. 13(b).

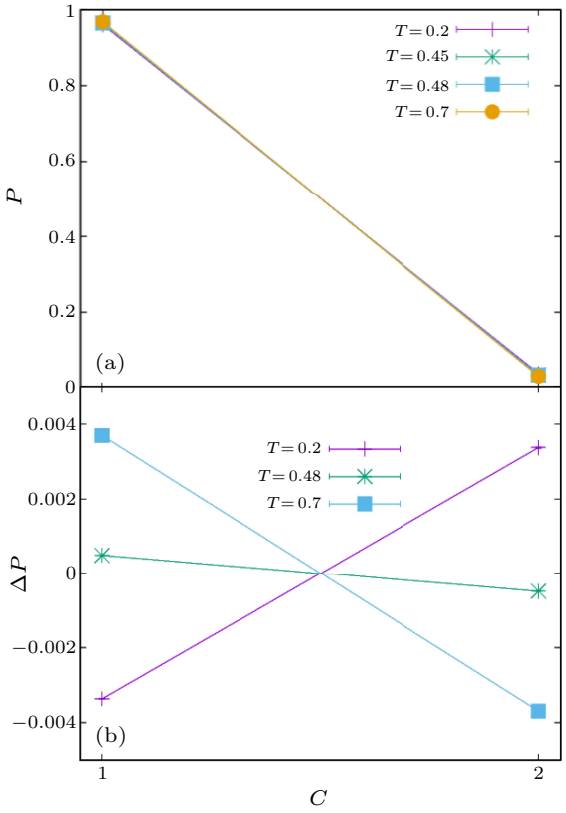


Fig. 13. Results illustrating the crossover behavior in the symmetric model at patch size $\theta = 10^\circ$ and $L = 64$. (a) Fraction P of disks belonging to clusters of size C with PP connections. (b) ΔP vs. C, with ΔP being the value of P after subtracting its value at the crossover temperature $T = 0.45$.

Interestingly, in the range $0^\circ < \theta \leq 30^\circ$, we find that, along the crossover curve, the inverse temperature $1/T$ increases with θ for the symmetric model, while it decreases with θ for the asymmetric model. We try to explain this difference by analytically calculating the heat capacity C_e of the models with two particles as follows.

For the asymmetric model, considering the occupation of an edge by two interacting particles in equilibrium, we derive the following partition function:

$$Z = 4\theta^2 e^{\beta\varepsilon} + [4 \times (180^\circ)^2 - 4\theta^2]. \tag{8}$$

Denoting $x = \beta\varepsilon$ and defining the specific heat as $C_e = (\beta^2/2)(\langle E^2\rangle - \langle E\rangle^2)$, we can reach

$$C_e = (x^2/2)\left[\frac{\theta^2 e^x}{\theta^2 e^x - \theta + (180^\circ)^2} - \frac{\theta^4 e^x}{\{\theta^2 e^x - \theta + (180^\circ)^2\}^2}\right]. \tag{9}$$

Then we solve the equation $\partial C_e/\partial x = 0$, and obtain the relationship between θ and the crossover $1/T$ (in units of k_B/ε)

as

$$\theta = \frac{180^\circ\sqrt{2+\frac{1}{T}}}{\sqrt{2-2\,\mathrm{e}^{1/T}+\frac{1}{T}+\frac{1}{T}\,\mathrm{e}^{1/T}}}. \tag{10}$$

We plot the above solutions of C_e and θ in Figs. 14(a) and 14(c), and find that the crossover $1/T$ decreases with θ in the range $0^\circ < \theta \leq 30^\circ$.

For the symmetric model, we can reach

$$\begin{aligned} Z = {} & [4(180^\circ)^2 - 8\times 180^\circ\theta + 8\theta^2]\,\mathrm{e}^{\beta\varepsilon} \\ & + 8\times(180^\circ)\theta - 8\theta^2. \end{aligned} \tag{11}$$

The heat capacity is derived to

$$\begin{aligned} C_\mathrm{e} &= (x^2/2)\left[\frac{A\,\mathrm{e}^x}{A\,\mathrm{e}^x - B} - \frac{A^2\,\mathrm{e}^{2x}}{(A\,\mathrm{e}^x - B)^2}\right], \\ A &= 4(180^\circ)^2 - 8\times 180^\circ\theta + 8\theta^2, \\ B &= 4\theta(360^\circ - 2\theta). \end{aligned} \tag{12}$$

The relation between $1/T$ and θ at crossover is obtained as

$$\begin{aligned} \theta &= 90^\circ \pm \frac{\sqrt{-8\,\mathrm{e}^{1/T}(180^\circ)^2(-2+\frac{1}{T})F + 4\times 180^\circ F^2}}{4F}, \\ F &= \left[2+\mathrm{e}^{1/T}(-2+\frac{1}{T})+\frac{1}{T}\right]. \end{aligned} \tag{13}$$

In the range $0^\circ < \theta \leq 30^\circ$, as plotted in Figs. 14(b) and 14(d), the above solutions show that the crossover $1/T$ increases with θ.

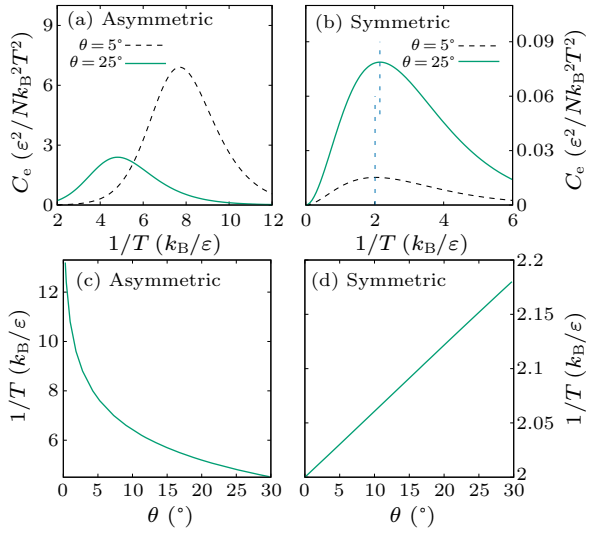


Fig. 14. Analytical results for two-particle systems. (a) C_e vs. $1/T$ for the asymmetric model, (b) C_e vs. $1/T$ for the symmetric model, (c) the crossover $1/T$ vs. θ for the asymmetric model, (d) the crossover $1/T$ vs. θ for the symmetric model.

Thus, the numerically found difference in the trend of the crossover lines of the two models could be qualitatively understood by the above theoretical analysis of the two-particle systems.

4. Discussion and conclusion

In summary, we have studied the phase behavior and percolation of an equilibrium system of symmetrically interacting Janus disks on the triangular lattice, and compared them with those of an asymmetrically interacting system. The phase diagrams for the symmetric and asymmetric models are shown in Figs. 3 and 4, respectively.

The phase diagram for the symmetric model is symmetric around the patch size $\theta = 90^\circ$ by definition. For patch sizes in the range $60^\circ < \theta < 120^\circ$, we find a continuous thermodynamic phase transition from a high-T disordered phase to a low-T orientationally ordered stripe phase. We also find that percolation in the stripe phase is anisotropic. These properties of the symmetric model are similar to those of the asymmetric model. In particular, we expect that the anisotropic percolation behavior can be understood by standard isotropic percolation using a nontrivial rescaling proposed in a recent work on the asymmetric model.[20]

We obtain several crossover curves for both the symmetric and asymmetric models, by identifying the peak of the specific heat C_e at fixed temperatures or patch sizes. These curves indicate crossovers between different structures. It is observed that the crossover behavior in the symmetric model is quite different from that of the asymmetric model. Main differences include: (i) There is a continuous crossover curve which spans the range $0^\circ < \theta \leq 90^\circ$ in the symmetric model, while there is no such curve in the asymmetric model. (ii) Along the crossover curve in the range $0^\circ < \theta \leq 30^\circ$, the value of $1/T$ increases with θ in the symmetric model, while it decreases with θ in the asymmetric model. These tendencies of $1/T$ vs. θ could be understood by analytically solving the two models with only two particles.

These results could provide useful references for studying more complex systems, such as asymmetric systems with nonzero PP and NN interactions, or systems with nonzero PN interactions. Since the results are obtained by triangular-lattice simulations of close-packed systems, it will be interesting to investigate whether and how the observed phenomena would change in continuum close-packed systems. It could also be interesting to study the phase behavior of Janus particles on other lattices. For example, when the patch sizes are small, in the limit $T \to 0$, all particles form dimers, and the models are equivalent with close-packed hard-core dimers on lattices.[34,35] While the classical dimer problem displays short-ranged correlations on the triangular lattice,[35] it displays critical (i.e., power-law) correlations on the square lattice.[34]

Acknowledgements

This work was supported by the National Natural Science Foundation of China (Grant No. 11905001). We acknowledge

the High-Performance Computing Platform of Anhui University for providing computing resources.

References

[1] Casagrande C and Veyssié M 1988 *C. R. Acad. Sci. (Paris)* **II-306** 1423
[2] Casagrande C, Fabre P, Raphal E and Veyssié M 1989 *Europhys. Lett.* **9** 251
[3] Lahann J 2011 *Small* **7** 1149
[4] Zhang J, Grzybowski B A and Granick S 2017 *Langmuir* **33** 6964
[5] Kirillova A, Marschelke C and Synytska A 2019 *ACS. Appl. Mater. Interfaces* **11** 9643
[6] Zhang X, Fu Q, Duan H, Song J and Yang H 2021 *ACS Nano* **15** 6147
[7] Chen Q, Bae S C and Granick S 2011 *Nature* **469** 381
[8] Mao X, Chen Q and Granick S 2013 *Nat. Mater.* **12** 217
[9] Jiang S, Yan J, Whitmer J K, Anthony S M, Luijten E and Granick S 2014 *Phys. Rev. Lett.* **112** 218301
[10] Rezvantalab H, Beltran-Villegas D J and Larson R G 2016 *Phys. Rev. Lett.* **117** 128001
[11] Huang Z, Zhu G, Chen P, Hou C and Yan L T 2019 *Phys. Rev. Lett.* **122** 198002
[12] Huang T, Han Y L and Chen Y 2020 *Soft Matter* **6** 3015
[13] Liang Y H, Ma B and Olvera de la Cruz M 2021 *Phys. Rev. E* **103** 062607
[14] Mitsumoto K and Yoshino H 2018 *Soft Matter* **14** 3919
[15] Shin H and Schweizer K S 2014 *Soft Matter* **10** 262
[16] Iwashita Y and Kimura Y 2014 *Soft Matter* **10** 7170
[17] Patrykiejew A and Rżysko W 2020 *Physica A* **548** 123883
[18] Patrykiejew A and Rżysko W 2021 *Physica A* **570** 125819, containing corrections to Ref. [17]
[19] Huang T, Zeng C H, Wang H, Chen Y and Han Y L 2022 *Phys. Rev. E* **106** 014612
[20] Hu H, Ziff R M and Deng Y J 2022 *Phys. Rev. Lett.* **129** 278002
[21] Wang Q C, He Z F, Wang J F and Hu H 2022 *Phys. Rev. E* **105** 034118
[22] Kern N and Frenkel D 2003 *J. Chem. Phys.* **118** 9882
[23] Jiang S and Granick S 2008 *Langmuir* **24** 2438
[24] Manousiouthakis V I and Deem M W 1999 *J. Chem. Phys.* **110** 2753
[25] Scullard C R and Ziff R M 2008 *Phys. Rev. Lett.* **100** 185701
[26] Scullard C R and Ziff R M 2010 *J. Stat. Mech.* P03021
[27] Scullard C R 2011 *J. Stat. Mech.* P09022
[28] Scullard C R and Jacobsen J L 2012 *J. Phys. A: Math Theor.* **45** 494004
[29] Mertens S and Ziff R M 2016 *Phys. Rev. E* **94** 062152
[30] Scullard C R and Jacobsen J L 2020 *Phys. Rev. Res.* **2** 012050
[31] Machta J, Choi Y S, Lucke A, Schweizer T and Chayes L M 1996 *Phys. Rev. E* **54** 1332
[32] Newman M E J and Ziff R M 2001 *Phys. Rev. E* **64** 016706
[33] Xu W H, Wang J F, Hu H and Deng Y J 2021 *Phys. Rev. E* **103** 022127
[34] Fisher M E and Stephenson J 1963 *Phys. Rev.* **132** 1411
[35] Fendley P, Moessner R and Sondhi S L 2002 *Phys. Rev. B* **66** 214513